Check for updates

Advanced Robotics Research

ADVANCED ROBOTICS RESEARCH Open Access

RESEARCH ARTICLE OPEN ACCESS

Distributed Micropneumatic Sensors for Soft Robots to Detect Touch and Pose

Vilma Lampinen[1] | Mika Pihlajamäki[1] | Md Nazmul Huda[2] | Veikko Sariola[1]

[1]Faculty of Medicine and Health Technology, Tampere University, Tampere, Finland | [2]Department of Engineering, Brunel University of London, Uxbridge, UK

Correspondence: Veikko Sariola (veikko.sariola@tuni.fi)

Received: 5 June 2026 | **Revised:** 21 September 2026 | **Accepted:** 1 October 2026

Keywords: microfluidics | pneumatic actuator | pneumatics | soft gripper | soft sensors

ABSTRACT

Soft robots benefit from their compliant materials, but the potential of safe and reliable operation remains limited without integration of strain and tactile sensors to detect contact, collisions, and robot pose. While humans achieve dexterous grasping through a dense distribution of mechanoreceptors in their hands, soft robotic grippers likewise need touch and pose sensing. Soft grippers often use pneumatic actuators, but integrating electrical or optical sensors to such actuators complicates their fabrication. Recently, we have reported a novel class of stretchable sensors, where the tactile pressure or strain measurement is based on measuring changes in airflow resistance caused by the deformation of a soft microchannel. These sensors are fabricated using identical techniques and materials as soft pneumatic actuators. In this work, we present a three-fingered soft gripper with 18 distributed micropneumatic sensors. Each finger consists of a pneumatic actuator and six micropneumatic sensors. We demonstrate that multichannel micropneumatic sensing enables reliable detection of finger pose and object contact, supporting object recognition during grasping. Overall, the work provides a solution for integrating touch and pose sensing into soft robots without requiring additional fabrication methods or materials beyond those used for pneumatic actuators.

1 | Introduction

Soft robots, fabricated from compliant, rubber-like materials, have emerged as a promising alternative to traditional rigid robots [1]. Soft robots are usually fabricated through casting or 3D-printing of elastomeric materials [2–4], and they are typically actuated using pneumatic or hydraulic systems [5–8] with pneumatic logic emerging as a promising control approach [9–11]. Their compliance limits the severity of accidental contact, such as unintended collisions or falls, making them particularly compelling for human–robot interaction [12, 13], wearable systems [14, 15], and the handling of fragile or irregularly shaped objects [6–8, 16] in agriculture and manufacturing. However, the promise of safety and reliable operation cannot be fully realized without tactile and strain sensors to detect contacts, collisions, and the pose of the robot because soft pneumatic actuators can still apply significant total contact forces (e.g., >100 N) [17], even if the contact pressure is evenly distributed.

Human hand, the pinnacle of tactile sensing, is highly innervated and contains approximately 17 000 cutaneous mechanoreceptors [18], which respond to mechanical stimuli such as contact, pressure, vibration, and skin deformation. Together, these sensory receptors enable precise object manipulation, texture discrimination, and stable grasping. Rather than relying on a single receptor type, the hand contains several classes of low-threshold mechanoreceptors distributed at different depths in the skin, each encoding complementary information. The resulting sensory signals are processed by the brain, which integrates inputs across receptor types and locations to detect both finger pose and external touch, enabling dexterous grasping.

This is an open access article under the terms of the Creative Commons Attribution License, which permits use, distribution and reproduction in any medium, provided the original work is properly cited.

© 2026 The Author(s). *Advanced Robotics Research* published by Wiley-VCH GmbH.

The lessons from the human hand suggest that soft robots would benefit from having multiple sensors, each at different locations and depths, with subsequent inference based on the processed multichannel sensor signals. While many sensorized soft grippers employ only a single sensing element per finger [19–22], multichannel sensing has also been implemented using soft or flexible electrical [23–25], optical [26–28], and magnetic sensors [29] integrated into the fingers or the palm of the gripper. However, their integration into soft pneumatic actuators requires additional transducers to convert signals across different energy domains, increasing system complexity and potential error sources. In addition, embedding conductive materials (e.g., liquid metals [30–32] or conductive nanomaterials [33, 34]) or optical waveguides [26, 27] into soft actuators complicates the fabrication process and can reduce the overall compliance of the finger. Moreover, the heterogeneous use of materials creates material interfaces that are prone to delamination and represent potential points of mechanical and functional failure.

Recently, we reported micropneumatic sensors [35], where we measure the airflow resistance of a soft micropneumatic channel. When the soft channel deforms, the airflow resistance changes. Our approach is distinct from measuring the pressure change in a closed soft elastomeric chamber [21, 36–38], using pneumatic bistable valves [39], or exploiting actuator pressure as a sensing signal [40]. Measuring pressure of a closed chamber is sensitive to any leakage and bistable valves provide only binary feedback, limiting their applicability for long-term measurements and continuous deformation or force magnitude sensing. We have demonstrated that our flow resistance measuring micropneumatic sensors are stable during long-term loading, show no hysteresis, and withstand up to 300% engineering strains, and can be used both as strain and tactile sensors [35, 41, 42]. The sensors exhibited negligible changes in output after 1000 cycles at 67% strain [35] and 5000 compression cycles at 1 N [41], demonstrating robustness under repeated mechanical loading. During long-term loading exceeding 12 h, only minor changes in sensor output were observed [35, 41, 42], which were primarily attributed to the viscoelastic behavior of the elastomeric material. The micropneumatic sensors are also suitable for measuring finger bending [35], as typical actuator bending induces only small strains. In addition, the micropneumatic channel is fabricated from the same materials used in soft pneumatic actuators and does not require additional transistors or power sources, simplifying the overall complexity of the device.

Although numerous sensorized soft grippers have been reported [43–46], relatively few utilize pneumatic sensing, and even fewer employ distributed pneumatic sensing along the active fingers of the gripper. This limited adoption motivates the development of distributed micropneumatic sensing for providing both tactile and proprioceptive information. Here, we report a three-fingered soft robotic gripper innervated with 18 distributed micropneumatic sensors to detect touch and pose (Figure 1a). A total of 18 sensors in a soft gripper represents the state-of-the-art in sensor integration into soft robots (Table 1). Each finger includes a pneumatic actuator and six micropneumatic channels (Figure 1b). One channel is embedded deeper within the finger to predominantly sense finger bending and deformation, while the remaining five channels are positioned close to the surface to measure contact and tactile forces (Figure 1d). The airflow resistance of each channel is measured using a pressure divider, analogous to a voltage divider in electronics (Figure 1c). We show that multichannel micropneumatic sensing enables simultaneous detection of finger pose and contact interactions, supporting object detection and recognition during grasping tasks (Figure 1e). Overall, this work shows that our micropneumatic sensing is a promising way to integrate multichannel touch and pose sensing into

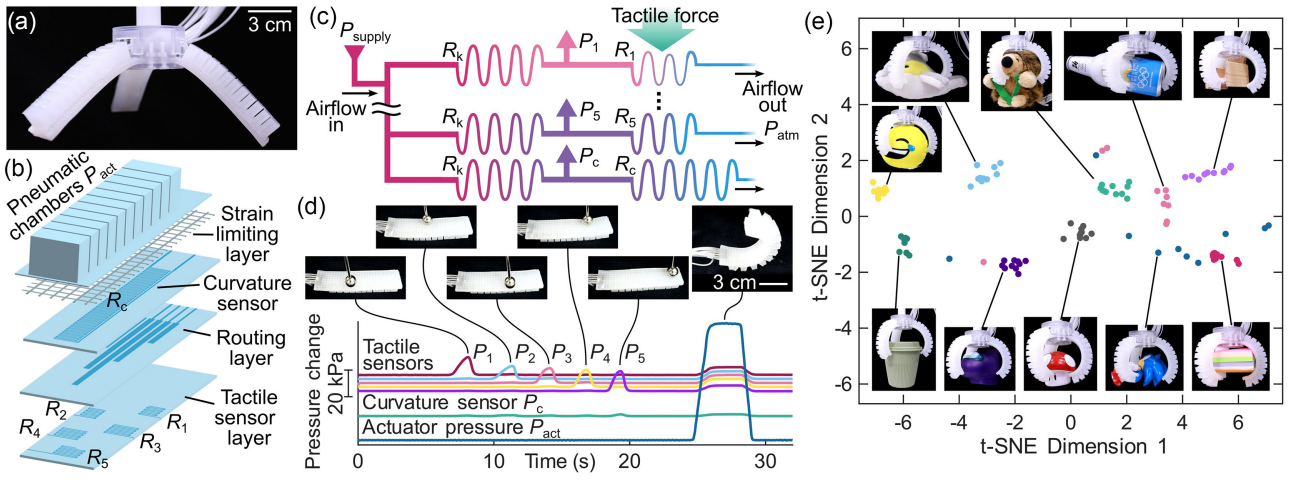


FIGURE 1 | Micropneumatically innervated soft gripper. (a) Photograph of the three-fingered pneumatic gripper with distributed micropneumatic sensors. (b) Schematic of the gripper finger with micropneumatic sensors in two layers for curvature (R_c) and tactile detection ($R_{1–5}$). (c) Circuit diagram of the micropneumatic sensors in one gripper finger. The color indicates the pressure at each point, ranging from light blue at low pressures through purple at intermediate pressures to pink at high pressures. The micropneumatic sensors can be considered as variable pneumatic resistors $R_{1–5,c}$ creating pressure dividers when connected in series with constant pneumatic resistors R_k. Supply pressure P_{supply} is applied to the circuit and each sensor is vented to atmospheric pressure P_{atm}. Pressures between the dividers $P_{1–5,c}$ are measured. When a tactile force is applied to the sensing channel, the channel deforms, resulting in an increase in airflow resistance and, consequently, the measured pressure. (d) Pressure change of each micropneumatic sensor and driving pressure of the actuator as the bottom of the finger is compressed from the tactile sensors one by one followed by a single bending event. (e) t-SNE visualization of the micropneumatic sensor data in object recognition experiment. Each object was picked by the gripper 10 times.

29439973, 0, Downloaded from https://advanced.onlinelibrary.wiley.com/doi/10.1002/adrr.70186 by NICE, National Institute for Health and Care Excellence, Wiley Online Library on [07/11/2026]. See the Terms and Conditions (https://onlinelibrary.wiley.com/terms-and-conditions) on Wiley Online Library for rules of use; OA articles are governed by the applicable Creative Commons License

TABLE 1 | Comparison of our micropneumatically innervated soft gripper to other grippers from the literature. To make meaningful comparisons between the different works, the table includes only soft fingered grippers that have multiple curvature and/or tactile sensors.

	Number of sensors						
Sensor type	Per finger	× Fingers	= Total	Recognition accuracy	Fabrication and materials	Notes	References
Resistive	2	4	8	94.5%	Flexible sensors embedded in elastomer	Object recognition	[24]
Resistive	2	2	4	N.R.	Microchannel filled with liquid metal	Curvature sensor located on top of pneumatic chambers	[23]
Resistive	4	3	12	N.R.	Microchannel filled with conductive ionogel	Curvature sensor located on top of pneumatic chambers, sensing regions across the finger bottom	[25]
Resistive & capacitive	4	3	12	98.64%	Ionic hydrogel	Machine-learning-based object recognition	[47]
Triboelectric	5	3	15	98.1%	Elastomer with Ni-fabric and copper electrodes	Four tactile sensors and one bending angle sensor	[48]
Magnetic	4	2	8	N.R.	Flexible printed circuit with a cracked ferrite film	Sensing regions across the finger bottom	[29]
Optical	2	5	10	~100% shape prediction with RGB camera	Polyurethane optical fibers with 3D-printed holders	Additional RGB camera and time-of-flight sensor integrated into the palm of the robot	[27]
Optical	3	3	9	98.077%	Polyurethane optical fibers in PDMS cladding	Shape recognition via LSTM deep learning	[28]
Pneumatic air chamber	6	2	12	N.R.	3D printing closed elastomeric and pneumatic cavities	Two passive sensorized compliant structures as the fingers	[49]
Pneumatic air chamber	2–3	5	14	N.R.	Multi-material 3D printing closed pneumatic chambers	Only tactile sensing, additional four tactile sensors in the palm of the gripper	[50]
Airflow resistance	**6**	**3**	**18**	**95%**	**Microchannel with airflow**	**Object detection, single-material sensing element**	**This work**

Note: Bold indicates values from this work.
Abbreviation: N.R., not reported.

soft robots without using any additional materials beyond those already used in the fabrication of the soft pneumatic actuators.

2 | Results

2.1 | Design and Working Principle of Micropneumatically Innervated Gripper

The fabricated soft gripper with distributed micropneumatic sensors has three pneumatic actuators as its fingers radiating outward with equal separation. The actuators consist of pneumatic chambers at the top, a glass fiber mesh as a strain-limiting layer in the middle, and the micropneumatic sensors at the bottom (Figure 1b). A custom 3D-printed centerpiece (Figure S3) holds the actuators together and contains all the pneumatic connections to the chambers of the actuators and their micropneumatic sensors. The gripper was attached to a vertical motor with a plastic screw, and all three fingers were actuated in unison by a shared pressure P_{act} supplied by an external pressure controller, making them open and close simultaneously.

Each finger of the gripper contains six micropneumatic sensors in the bottom of the finger in two layers (Figure 1a,b): one

29439973, 0, Downloaded from https://advanced.onlinelibrary.wiley.com/doi/10.1002/adrr.70186 by NICE, National Institute for Health and Care Excellence, Wiley Online Library on [07/11/2026]. See the Terms and Conditions (https://onlinelibrary.wiley.com/terms-and-conditions) on Wiley Online Library for rules of use; OA articles are governed by the applicable Creative Commons License

curvature sensor across the full length of the finger and five tactile sensors closer to the surface, each covering different area of the surface (Figure 1a). The curvature sensor is more responsive to the bending of the entire finger, while tactile sensors are more responsive to local touch and bending in different regions of the finger. However, the signals are coupled: bending of the finger affects all the tactile sensor signals, and pressing the finger also affects the curvature sensor signal.

The width and height of the sensing channels are both 200 µm, while the channel length varies between sensors (see Section 4). Routing layer between the curvature sensor and tactile sensors provides inlet channels to the tactile sensors (Figure 1b). The entire finger with the sensors is fabricated from soft polydimethylsiloxane elastomer (Shore A hardness 30) by casting it into 3D-printed molds. There is a small airflow through the microchannels, and the flow resistance of each sensing channel changes when it deforms due to bending of the finger or tactile forces.

The change of the flow resistance of the micropneumatic sensor is measured with a pressure divider that is analogous to a voltage divider (Figure 1c) [35]. Each sensor channel is connected in series to a constant pneumatic resistor (a meandering microchannel external to the robot, R_k in Figure 1c). Constant positive supply pressure $P_{supply} = 60$ kPa is applied over the channels while the channels are vented to atmospheric pressure P_{atm}. Pressures $P_{1\text{–}5,c}$ measured from the junctions between the constant resistors and sensing channels depend on the flow resistance of the sensing channels. We calculate the change in these pressures as $\Delta P = P - P_0$, where P_0 is the initial sensor reading with the finger in neutral state.

2.2 | Touch and Pose Sensing

To demonstrate that the micropneumatic sensors can be used to detect touch and pose, the sensor responses to different stimuli were tested with a single finger. First, the bottom of the finger was compressed from five different points with a spherical probe (Ø1.27 cm) by hand, corresponding to the locations of the five tactile sensors, after which the actuator was inflated once (Figure 1d and Video S1). The sensor responses $P_{1\text{–}5,c}$ and the actuator pressure P_{act} are plotted as a function of time in Figure 1d. The tactile sensor immediately below the compressing probe deforms the most, giving the highest response, but the curvature sensor underneath also responds slightly. When bending the finger, all the sensors respond. From these data, we conclude that the distributed micropneumatic sensors can be used to detect both the bending of the finger and touch on its surface, but the signals are coupled.

To further study the touch sensitivity of the tactile sensors, the bottom of the finger was compressed with the spherical probe (Ø1.27 cm, 3 N force) from 33 different points (Figure 2a). For each point, we calculated the sensitivity (units: N^{-1}) of the five different tactile sensors and plotted heat maps of the sensitivity for the five sensors in Figure 2b. The sensitivities were obtained by plotting the relative sensor response $\Delta P/P_0$ as a function of the compression force (Figure 2c) and fitting a linear line to this data; the sensitivity is then the slope of this linear fit. Note that the sensor response is not perfectly linear (Figure 2c), so these values slightly depend on the range of force tested.

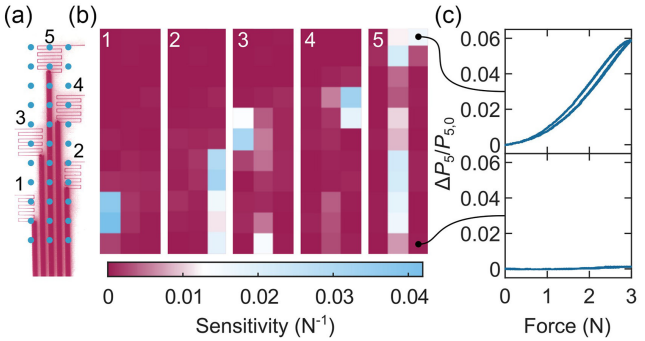


FIGURE 2 | Touch sensing. (a) Photograph of the tactile sensors and routing layer, overlayed with a grid showing the compression points. The channels were filled with dyed liquid to visualize them. (b) Sensitivity of all five different tactile sensors as a function of the compression point when compressed with 3 N force from those points. (c) Insets showing the force-sensor response curves for two of the compression points in the same experiment. The sensitivity is the slope of a linear fitted line to this data.

In the sensitivity maps (Figure 2b), we see a clear response when the compression point is right above the tactile sensor but also when the compression point is above the routing channel of the sensor. This can be clearly seen in sensor 5: the middle column of the compression points is directly on its routing channel, that is responding to every contact. The routing channels are like nerves in the human body: their main function is to transmit signals through the body, but they also respond when directly stimulated. Like the ulnar nerve at the elbow produces a sensation when struck ("funny bone"), the routing channel also reacts to compression. The same effect can be seen in sensors 2–4, but to a lesser degree. Taking the data in Figure 2 as a whole, it is clear that the tactile sensor response corresponds to the sensing and routing channel design on the surface.

The tactile sensors exhibited a maximum hysteresis of 8.7% during five repeated 3 N compression cycles, with part of the hysteresis likely arising from the viscoelastic behavior of the elastomer (Figure S1). Figures 2c and S1 also show that the response of the tactile sensors is sigmoidal, increasing superlinearly at low force levels and sublinearly at higher forces when the microchannel is approaching full closure and the sensor output begins to saturate. Hence, the sensitivity of the sensor is highest in the intermediate region of the response curve and lower at both low and high forces. The onset of saturation near 3 N suggests that the operational force range of the tactile sensors extends only slightly beyond the tested range.

To show that we can use the sensors to detect the pose of the finger even when it is colliding with an object, an obstacle was placed in front of the finger, and the finger was bent by pressurizing the actuators with $P_{act} = 85$ kPa. The experiment was repeated 24 times, where the position of the obstacle was varied. As ground truth, the 2D shape of the bottom edge of the finger was captured using a side-view camera and machine vision. We then trained a simple feedforward neural network to reconstruct the side-view shape and bottom edge of the finger with the data from the micropneumatic sensors and actuator pressure as input. The output of the network was the coordinates of points sampled along the bottom edge of the finger, representing its 2D

29439973, 0, Downloaded from https://advanced.onlinelibrary.wiley.com/doi/10.1002/adrr.70186 by NICE, National Institute for Health and Care Excellence, Wiley Online Library on [07/11/2026]. See the Terms and Conditions (https://onlinelibrary.wiley.com/terms-and-conditions) on Wiley Online Library for rules of use; OA articles are governed by the applicable Creative Commons License

shape as observed by the side-view camera (see Section 4). The cross-validation was done in a leave-one-out manner, where for each of the 24 experiments, a new network was trained with the one experiment used only as the validation data, and the rest of the experiments ($N=23$) as the training data. Furthermore, as a control experiment, another set of the networks was trained using only the actuator pressure P_{act} as its input. The purpose of this was to evaluate the contribution of the micropneumatic sensors to the shape reconstruction performance.

The results are shown in Figure 3 with video snapshots from the experiments. The pose of the finger predicted based on the data from the micropneumatic sensors and the pressure of the actuator (*in dashed yellow*) clearly follows the machine-vision-detected bottom edge of the finger (*in solid pink*), with the two curves almost completely overlapping in all 24 cases. In comparison, the reconstruction based on only the actuator pressure P_{act} (*in solid blue*) is practically identical in all cases regardless of the true pose of the finger and differs significantly from the machine-vision-detected ground truth. This is expected: without any sensor information, the neural network always predicts average bending, sometimes overestimating and sometimes underestimating it, depending on the location of the obstacle. From these results, we conclude that the sensors are necessary to accurately detect the true pose of the finger when it collides with an obstacle.

2.3 | Object Detection

As the outputs of the micropneumatic sensors depend on pose of the fingers and how they touch external objects, we tested if the gripper with the distributed micropeumatic sensors can detect the type of the object being picked. We picked 10 differently shaped objects with the gripper while recording the sensor outputs, and each object was picked 10 times. The results are presented in Figures 1e and 4 as two-dimensional t-distributed stochastic neighbor embedding (t-SNE). The t-SNE is used for visualization of the sensor data structure rather than for quantitative classification. The full data set is 18-dimensional, with six sensors in each of the three fingers, with the sensor values sampled at the time when the gripper has fully closed; however, in Figure 4, we also show the t-SNE constructed by only using subsets of the sensor channels. Note that although Figure 4d uses the same 18-dimensional data as Figure 1e, the resulting t-SNE visualizations slightly differ due to the stochastic nature of t-SNE. t-SNE keeps the local cluster structure fairly consistent, but there are global variations depending on the random initialization of the algorithm.

The plots in Figures 1e and 4d reveal clear separations between the classes, suggesting that the sensor data is highly structured and the objects can be recognized from each other. A couple of objects (bottle and figurine with blue hair, shown *in light pink* and *in dark blue*, respectively) have some outliers from their clusters, which we attribute to variations in the picking pose or sliding of the object during picking compared to other trials. Overall, this experiment demonstrates that the three-fingered gripper with distributed micropneumatic sensors can distinguish between different picked objects based on the resulting sensor responses.

The classes become more clearly separated when more sensor channels are used in the t-SNE analysis (Figure 4). In the first plot, only data from the curvature sensors (P_c) of the three fingers was used, making the sensor data 3-dimensional. The subsequent plots were obtained by progressively including more tactile sensor channels in the t-SNE mapping, with the last plot using all the sensor data, making it 18-dimensional. It can be seen from Figure 4 that as more sensor channels are included, the classes become progressively clearer and better separated. This suggests that the curvature sensor alone is not sufficient for reliable object detection, but with the help of the tactile sensors, different objects can be better recognized, and increasing the number of tactile sensors enhances the ability of the gripper to distinguish the picked objects.

For quantitative evaluation, a k-nearest neighbors (k-NN) classifier was trained using the sensor data from the object-picking experiment. The performance of the classifier was evaluated using leave-one-out cross-validation. Figure 5a shows the recognition

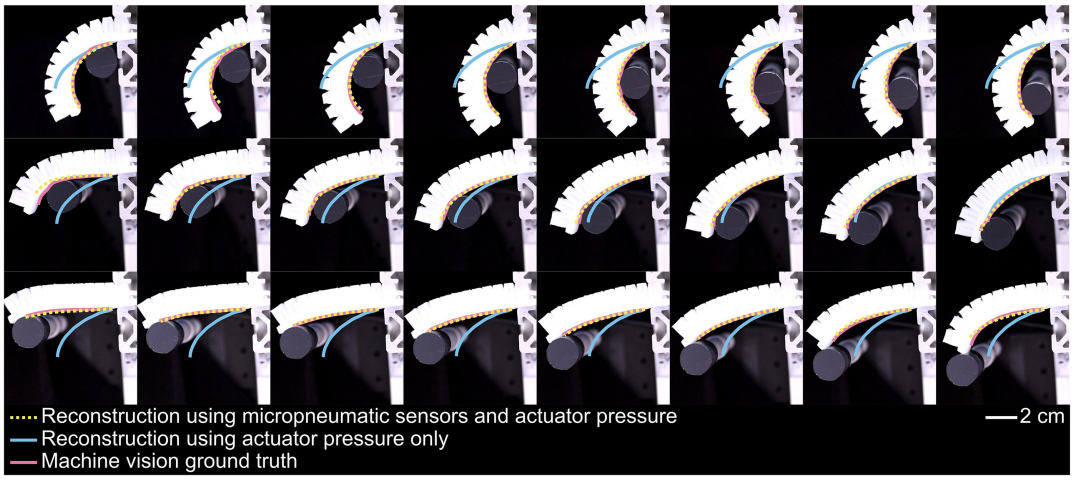


FIGURE 3 | Pose detection. Photographs of the micropneumatically innervated finger colliding with an obstacle. The obstacle is positioned at different locations to restrict the motion of the finger. The photographs are overlaid with machine-vision-detected shape of the finger (ground-truth, *in solid pink*), reconstructions based on output of the micropneumatic sensors and the pressure of the actuator (*in dashed yellow*), and reconstructions based on only the pressure of the actuator (*in solid blue*).

29439973, 0, Downloaded from https://advanced.onlinelibrary.wiley.com/doi/10.1002/adrr.70186 by NICE, National Institute for Health and Care Excellence, Wiley Online Library on [07/11/2026]. See the Terms and Conditions (https://onlinelibrary.wiley.com/terms-and-conditions) on Wiley Online Library for rules of use; OA articles are governed by the applicable Creative Commons License

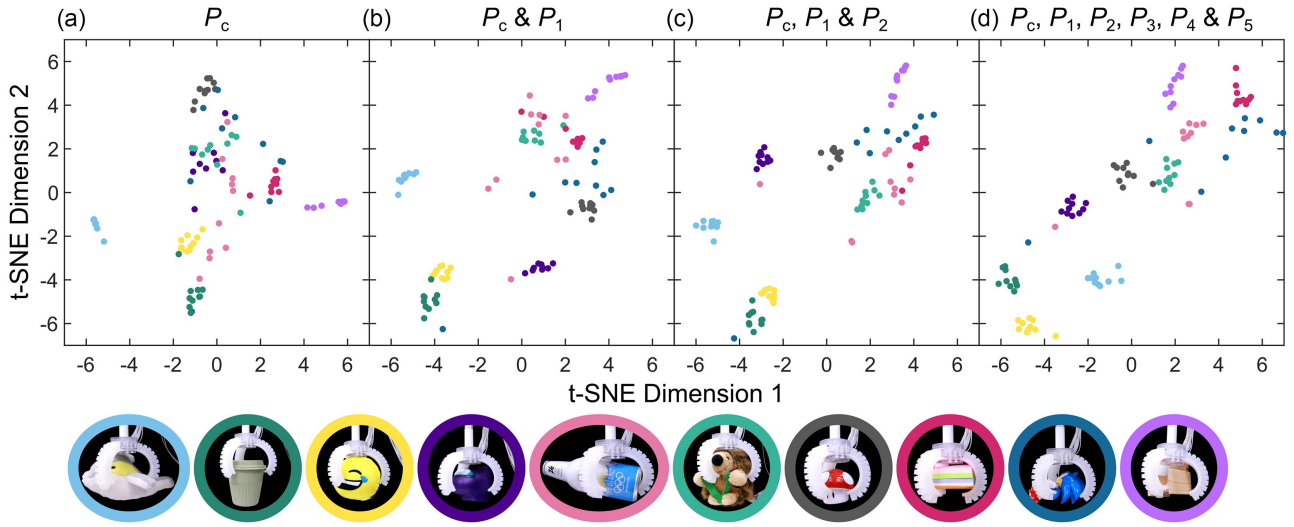


FIGURE 4 | t-SNE visualizations of sensor data collected during object-picking experiment using different subsets of the distributed micropneumatic sensors. The t-SNE data included: (a) only data from the curvature sensors (P_c; 3-dimensional data, as there are three fingers); (b) data from the curvature sensors and first tactile sensors (P_c and P_1; 6-dimensional data); (c) data from the curvature sensors and first two tactile sensors (P_c, P_1, and P_2; 9-dimensional data); and (d) data from all the sensors (P_c, P_{1-5}; 18-dimensional data).

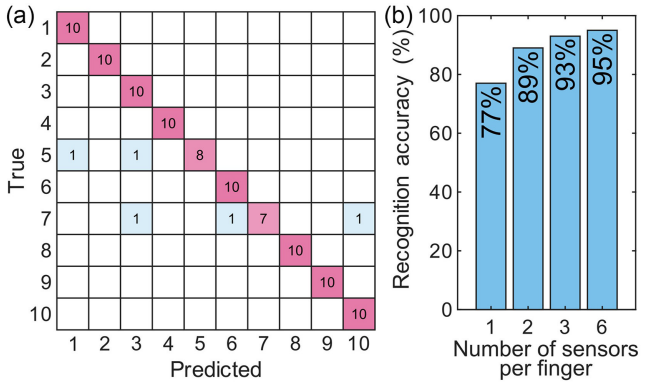


FIGURE 5 | Object recognition. (a) Confusion matrix of object recognition from sensor data using *k*-NN classifier when 10 different objects were picked 10 times each. Numbers correspond to object classes: (1) purple toy, (2) dolphin, (3) hedgehog, (4) post-it cube, (5) bottle, (6) mushroom, (7) figurine with blue hair, (8) smiley ball, (9) takeaway cup, and (10) doll chair. (b) Overall object recognition accuracy using data of different number of sensors on the fingers similarly as in Figure 4: (1) only data from the curvature sensors (P_c); (2) data from the curvature sensors and first tactile sensors (P_c and P_1); (3) data from the curvature sensors and first two tactile sensors (P_c, P_{1-2}); and (6) data from all the sensors (P_c, P_{1-5}).

confusion matrix obtained from the *k*-NN classifier when using data from all 18 sensors. Most objects are located along the diagonal, indicating correct recognition, while figurine with blue hair and the bottle are misclassified a couple of times, seen also as outliers from their clusters in t-SNE visualization (Figures 1e and 4d). The accuracy of the object recognition is 95% (Figure 5b) when the data from sensors including the curvature sensors and all tactile sensors are used. Using only the curvature sensor data results in an accuracy of 77%, which increases to 89% and 93% as more tactile sensors are progressively included, following the same trend shown in Figure 4. These results demonstrate that increasing the number of sensors improves the ability of the gripper to distinguish between different objects.

3 | Discussion and Conclusions

We integrated a total of 18 micropneumatic sensors into a three-fingered soft pneumatic gripper. We showed that the sensors can be used to both detect touch and pose of the gripper fingers, and that the sensors can be used to detect objects picked by the gripper.

Table 1 compares our work with previously reported soft robotic grippers that have multiple sensors distributed along their fingers. Six sensors per finger and 18 sensors in total are both on par with the state-of-the-art in terms of number of sensors: to our knowledge, no soft robotic gripper with more sensors has been reported, regardless of the sensing method used. However, our solution is unique as it is based on micropneumatic sensors measuring airflow resistance, with the distinct advantage of being based on identical fabrication methods and materials as the pneumatic actuators themselves [35], making it easy to integrate sensors into existing designs, and avoiding issues with distinct material interfaces [51].

The closest works in terms of object detection come from Zhou et al. [47] and Homberg et al. [24], but those works were based on electrical resistive or capacitive sensors, and had fewer sensors than our gripper. The data in Figures 4 and 5 show that having more sensors is advantageous for object recognition.

Sensing performance of micropneumatic tactile sensors is influenced by the nonlinear response of the deformable microchannels and by the viscoelastic nature of the elastomeric materials. The long-term stability of the sensing system is ultimately limited by the durability of the elastomeric materials used to fabricate the sensors. Silicone elastomers are known to exhibit viscoelastic effects, creep, stress relaxation, and eventually fatigue under prolonged loading. However, in the experiments conducted in our previous studies [35, 41], the micropneumatic sensors have shown stable response under long-term steady and dynamic measurements. As the cyclic tests involved thousands of consecutive cycles at strain levels exceeding those expected during typical gripper

29439973, 0, Downloaded from https://advanced.onlinelibrary.wiley.com/doi/10.1002/adrr.70186 by NICE, National Institute for Health and Care Excellence, Wiley Online Library on [07/11/2026]. See the Terms and Conditions (https://onlinelibrary.wiley.com/terms-and-conditions) on Wiley Online Library for rules of use; OA articles are governed by the applicable Creative Commons License

operation, sensor durability is unlikely to be a primary limitation in practical soft robotic applications.

In addition, temperature variations may influence the sensor response through changes in air viscosity and density as well as in mechanical properties of the elastomer. In our previous work [42], a 19.5% decrement of sensor response was observed at the sensor was heated from 30 °C up to 100 °C, suggesting that temperature compensation may be sufficient for applications with large temperature variations. Overall, our previous results indicate that micropneumatic sensors can provide reliable sensing performance in applications involving repeated mechanical loading and moderate environmental variations.

There are a few outstanding issues with our distributed micropneumatic sensors that could be improved upon. One is the coupling between curvature and tactile sensing. Separating these sensing modalities into soft structures is challenging because localized contact forces generate strain fields that propagate through the bulk material. As a result, sensors located beside or deep below the contact point may still have some response to localized compression, as we have shown.

First approach to reducing this effect would be to improve the sensor placement. On one hand, placing the tactile sensing channels as close to the surface as possible will make them more sensitive to tactile contact, as the strains are the largest below the contact point, close to the surface. On the other hand, placing the curvature sensors deeper within the structure makes them less sensitive to touch, but they still respond to global deformations such as bending. In some applications, the curvature sensor could even be placed on top of the pneumatic chambers, opposite from the primary gripping surface on the bottom side of the finger, if the robot designer can reasonably expect that the top side of the pneumatic chambers will not collide with anything.

The second approach to minimize sensor coupling is through differential sensing approaches where the measured value is not the output of a single sensor but a difference or a ratio of multiple sensor outputs. To minimize the number of external pressure lines, such a differential measurement could be implemented using a pneumatic Wheatstone bridge [52]. With these configurations, the sensitivity to specific deformation modes could be enhanced while suppressing others. However, because soft actuators can undergo large deformations and micropneumatic sensors have nonlinear responses, some degree of signal processing would likely still be required.

The final approach would be through signal processing, with linear decoupling matrices or nonlinear methods, such as the neural networks that we used in Figure 3. The input to the decoupler is the sensor readings, and the output would be the decoupled values of bending and tactile pressures. Calibration experiments were then be used to find the parameters of these decoupling models. Once decoupled, the bending and the contact pressures could be observed and thus controlled individually.

Another problem with our current design is that the routing channels also respond to the tactile pressure (Figure 2). For easy interpretation of the tactile sensor signals, it would be preferable to have the tactile sensors only respond to local pressures. This phenomenon might be avoidable by locating the routing channels deeper inside the robot. Another option would be making them from a stiffer material, but the stiffness cannot be increased too much without compromising the deformability of the finger. Finally, one option is to locate the routing channels to the neutral plane of the bending as a part of the strain-limiting layer. This would require fabricating a structured strain-limiting layer as opposed to the glass fiber mesh we currently use as the strain-limiting layer.

Future work could investigate differential micropneumatic sensing architectures and improved routing channel designs to reduce coupling between tactile and curvature sensing and to minimize the contribution of routing channels to the sensor output. Another promising direction is the use of the proposed sensor system in closed-loop grasping and manipulation tasks. Previous studies have demonstrated pressure regulation using micropneumatic sensors and pneumatic bistable valves within the same pneumatic circuit [53], suggesting that similar approaches could be extended to closed-loop grasping and object manipulation.

Another area for future work would be to better distribute the sensors throughout the finger. Currently, the sensors are located near the bottom surface, and none are positioned at the front tip of the finger or at the top of the pneumatic chambers. In the future, this could be addressed by developing a fabrication method to create true 3D micropneumatic channel networks, although practical approaches for reliably producing 3D channels from soft materials remain an open question.

Finally, while we have demonstrated 6 sensors per finger, which is comparable to the state-of-the-art in soft robot sensor integration, this is still an order of magnitude less than the 17 000 low-threshold mechanoreceptors humans have in their hands [18], with approximately 5000 of these already just in the fingertips. Assuming 3000 channels per finger would have to be routed through a 1 mm × 10 mm cross-sectional area, this would leave approximately 3000 μm^2 per channel, which should include the walls of the channel and the channel itself. Assuming the channels are square, this would correspond to ≈60 µm. Fabricating soft channels this small is entirely plausible, but measuring the pressures from so many parallel channels would present an immense practical challenge. Sparse sensing strategies [42] and fluidic sensing strategies employing time dynamics of the sensor response [54] could provide a path forward without increasing the number of sensors significantly.

To conclude, this work demonstrates multichannel micropneumatic sensing in a three-fingered soft robotic gripper for detecting finger pose and tactile contact without introducing additional materials beyond those already used for soft pneumatic actuation of the fingers. The use of multiple micropneumatic sensors in the gripper fingers provides the ability to distinguish between different grasped objects based on the sensor responses. The work advances soft robotic grippers toward fully pneumatic systems capable of safe and reliable operation through the detection of contact events, collisions, and gripper pose. Overall, our micropneumatic sensing enables integrated touch and pose perception in soft grippers for object detection without compromising compliance or fabrication simplicity.

29439973, 0, Downloaded from https://advanced.onlinelibrary.wiley.com/doi/10.1002/adrr.70186 by NICE, National Institute for Health and Care Excellence, Wiley Online Library on [07/11/2026]. See the Terms and Conditions (https://onlinelibrary.wiley.com/terms-and-conditions) on Wiley Online Library for rules of use; OA articles are governed by the applicable Creative Commons License

4 | Experimental Section

4.1 | Sensor Designs and Fabrication

Detailed drawings of the sensor designs are in Figure S2. The curvature sensor contains a meandering microchannel in one layer, while the tactile sensors have a routing layer providing inlets for the actual sensing channels. The length of the curvature sensing channel is ~760 mm with 90 turns and a cross-sectional area of 200 μm × 200 μm.

In the routing layer, there is a straight inlet channel for each of the tactile sensors (width: 400 μm, height: 400 μm, and inlet length: 35–80 mm depending on the location of the sensor). The tactile sensors closer to the inlet are slightly smaller, so that those sensing channels do not overlap with the routing channels. The tactile sensor sensing channels have 8 turns and the length of the channel varies between sensors. Sensors 1 and 2 (Figure 1b) have a length of 45 mm; sensors 3 and 4 have a length of 74 mm; and sensor 5 has a length of 69 mm. The width and height of all the sensing channels were 200 μm.

The sensors were fabricated layer-by-layer from Dragon Skin 30 elastomer (Smooth-On, Shore A hardness 30). A schematic of the entire fabrication process is shown in Figure S3. The layers with microchannels were fabricated by casting the elastomer into 3D-printed molds (Clear resin, Form 3BL, Formlabs). Throughout the fabrication process, we used a thin layer of spin-coated elastomer as an adhesive to bond layers together. The adhesive was partially cured before bonding the layers.

First, the cast layer with the tactile sensors was demolded and its flat backside was bonded against the backside of a cast layer with the routing channels. After bonding, vias connecting the channels in the both layers were pierced with a needle, and flat elastomer layers were bonded on both sides of the stack to serve as lids to close the channels. Next, the curvature sensor was cast and bonded to a lid to close the channel. The closed curvature sensor was then bonded to the previously fabricated stack of tactile sensors and routing channels. Finally, the entire stack with channels in three layers was cut to shape, revealing the inlets and outlets of the channels.

4.2 | Actuator and Gripper Fabrication

The pneumatic actuator was fabricated following the process adapted from Soft Robotics Toolkit [55]. Detailed drawings and dimensions of the actuator are presented in Figure S3. The chambers of the actuator were cast from Dragon Skin 30 in a 3D-printed mold made from polylactic acid (PLA, Prusa I3 MK3, Prusa Research). A glass fiber mesh was placed on top of the previously fabricated elastomer stack with the sensors, and a thin layer of uncured elastomer was evenly spread over it. The demolded pneumatic chambers were then placed on top (Figure S3). Finally, an air inlet was created in the first pneumatic chamber using a biopsy punch, and a tube was connected to it.

Three micropneumatically innervated fingers were fabricated for the soft gripper. A custom-made 3D-printed (Clear resin, Form 3BL, Formlabs) center-piece connected the fingers together and provided pneumatic connections from the measurement setup to the actuators and the micropneumatic sensors. Detailed drawings of the centerpiece and the gripper are provided in Figure S4. For the object recognition experiments, the gripper was mounted to a vertical motor (TA.XT Plus, Stable Micro Systems) with a plastic screw and the target objects were placed under the gripper manually for the picking.

4.3 | Experimental Setup

Schematic of the experimental setup is shown in Figure S5. Pressure sensors (015PDAA5, Honeywell, 15 PSI Differential 5 V) measured the pressures $P_{1-5,c}$ between the sensors and their constant pneumatic resistors (Figure 1c). The constant pneumatic resistors are microchannels (width: 200 μm, height: 200 μm, and length: 165 mm with 6 turns) fabricated from Dragon Skin 30 with same procedure as the sensing channels earlier. The pressure applied to the pneumatic circuitry P_{supply} was measured with the same pressure sensor. All pneumatic connections between the micropneumatic sensors and the measurement system were made from silicone tubes and plastic splitters. Pressure sensor data was acquired via a data acquisition device (USB-6255, National Instruments). For tactile sensor characterizations, a mechanical tester (TA.XT Plus, Stable Micro Systems) was used to compress the bottom of the actuator with a spherical probe (P/0.5S, Ø1.27 cm ball, Stable Micro Systems).

Pneumatic control board (Soft Robotics Toolkit [55]) was used to control the pneumatic actuators and soft gripper: solenoid valve (VQ11OU-5 M, SMC) was driven by an Arduino MEGA 2560 microcontroller using 56 Hz pulse-width modulation, with pressure regulated by adjusting the duty cycle of the solenoid valve. The Arduino was operated via custom MATLAB scripts. A pressure sensor (100PGAA5, Honeywell, 100 PSI GAGE 5 V) measured the pressure inside the pneumatic actuators and the data was recorded with the data acquisition device (USB-6255, National Instruments). The pressure data was recorded at a sampling frequency of 2 kHz in all experiments. A digital camera (Canon, EOS 5D Mark IV) was set up to capture video of the single finger in Figure 3 and closing gripper in grasping experiments.

4.4 | Pose Reconstruction

The pose reconstruction in Figure 3 was made as follows. Machine vision was used to obtain 20 equally spaced points along the bottom edge of the actuator in each video frame (25 FPS), with the first point manually initialized in the first frame of each experiment. For subsequent frames, the same bottom reference point was used, and the point locations were automatically updated using the same image-processing procedure. The recorded data from the micropneumatic sensors was temporally aligned with the machine vision result to obtain corresponding input-output pairs for neural network training and validation. A simple feedforward neural network was trained on the data, with the micropneumatic sensor signals $P_{1-5,c}$ and actuator pressure P_{act} as its inputs and the curve point coordinates as its outputs. The network had one hidden layer with 10 neurons. The network was implemented in MATLAB, using function `feedforwardnet`. Before network training, the micropneumatic sensor signals and the actuator

29439973, 0, Downloaded from https://advanced.onlinelibrary.wiley.com/doi/10.1002/adrr.70186 by NICE, National Institute for Health and Care Excellence, Wiley Online Library on [07/11/2026]. See the Terms and Conditions (https://onlinelibrary.wiley.com/terms-and-conditions) on Wiley Online Library for rules of use; OA articles are governed by the applicable Creative Commons License

pressure were normalized to zero mean and unit standard deviation, with each sensor channel normalized independently. The machine-vision-based point coordinates were similarly standardized and subsequently transformed using principal component analysis, retaining the first five principal components. For each of the 24 experiments, a separate network was trained using a leave-one-out cross-validation approach, where the target experiment was used only for validation and the remaining 23 experiments formed the training data. Networks were also trained using only the actuator pressure P_{act} as input to evaluate the contribution of the micropneumatic sensors beyond actuator pressure alone.

4.5 | Object Detection

In the object detection experiment (Figures 1e and 4), ten objects with distinct shapes were grasped using the gripper, with each object picked ten times from the position. The resulting sensor dataset was 18-dimensional, comprising six micropneumatical sensor channels from each of the three fingers. For each grasp, sensor values at full gripper closure were used for analysis. In data processing, the sensor data from ten objects, each grasped 10 times, were reshaped into a set of 100 feature vectors. The sensor data was visualized using the t-SNE with standardized Euclidean distance, using MATLAB function `tsne`. k-NN classifier ($k = 3$) was trained using MATLAB function `fitcknn` and evaluated using leave-one-out cross-validation. In each iteration, one grasping event was left out for testing, and its object class was predicted using a classifier trained on the remaining 99 events.

Author Contributions

V.L. and M.P. planned and conducted the experiments. V.S. and M.N.H. conceived the research and supervised the study. All authors discussed the results. V.L. and V.S. wrote the manuscript.

Acknowledgments

The work was supported by the Research Council of Finland (grants #343408 and #373636); the Doctoral Programme in Medicine, Biosciences, and Biomedical Engineering of Tampere University; and Brunel University of London.

Funding

This study was supported by the Research Council of Finland (343408 and 373636), Doctoral Programme in Medicine, Biosciences, and Biomedical Engineering of Tampere University, and Brunel University of London.

Conflicts of Interest

The authors declare no conflicts of interest.

Data Availability Statement

The data generated and analyzed during the study and the scripts used to analyze the data are available from Zenodo (https://doi.org/10.5281/zenodo.23264495), reference number 23264495.

References

1. D. Rus and M. T. Tolley, "Design, Fabrication and Control of Soft Robots," *Nature* 521 (2015): 467–475, https://doi.org/10.1038/nature14543.

2. R. F. Shepherd, F. Ilievski, W. Choi, et al., "Multigait Soft Robot," *Proceedings of the National Academy of Sciences* 108, no. 51 (2011): 20400–20403, https://doi.org/10.1073/pnas.1116564108.

3. F. Ilievski, A. D. Mazzeo, R. F. Shepherd, X. Chen, and G. M. Whitesides, "Soft Robotics for Chemists," *Angewandte Chemie International Edition* 50, no. 8 (2011): 1890–1895, https://doi.org/10.1002/anie.v50.8.

4. N. W. Bartlett, M. T. Tolley, J. T. B. Overvelde, et al., "A 3D-Printed, Functionally Graded Soft Robot Powered by Combustion," *Science* 349, no. 6244 (2015): 161–165, https://doi.org/10.1126/SCIENCE.AAB0129.

5. B. Mosadegh, P. Polygerinos, C. Keplinger, et al., "Pneumatic Networks for Soft Robotics That Actuate Rapidly," *Advanced Functional Materials* 24, no. 15 (2014): 2163–2170, https://doi.org/10.1002/ADFM.201303288.

6. R. V. Martinez, J. L. Branch, C. R. Fish, et al., "Robotic Tentacles With Three-Dimensional Mobility Based on Flexible Elastomers," *Advanced Materials* 25, no. 2 (2013): 205–212, https://doi.org/10.1002/ADMA.201203002.

7. S. Zaidi, M. Maselli, C. Laschi, and M. Cianchetti, "Actuation Technologies for Soft Robot Grippers and Manipulators: A Review," *Current Robotics Reports* 2, no. 3 (2021): 355–369, https://doi.org/10.1007/s43154-021-00054-5.

8. N. Zhang, J. Ren, Y. Dong, et al., "Soft Robotic Hand With Tactile Palm-Finger Coordination," *Nature Communications* 16, no. 1 (2025): 2395, https://doi.org/10.1038/s41467-025-57741-6.

9. M. Wehner, R. L. Truby, D. J. Fitzgerald, et al., "An Integrated Design and Fabrication Strategy for Entirely Soft, Autonomous Robots," *Nature* 536, no. 7617 (2016): 451–455, https://doi.org/10.1038/nature19100.

10. D. Drotman, S. Jadhav, D. Sharp, C. Chan, and M. T. Tolley, "Electronics-Free Pneumatic Circuits for Controlling Soft-Legged Robots," *Science Robotics* 6, no. 51 (2021): eaay2627, https://doi.org/10.1126/scirobotics.aay2627.

11. E. Gallardo Hevia, C. M. McCann, M. Bell, et al., "High-Gain Microfluidic Amplifiers: The Bridge Between Microfluidic Controllers and Fluidic Soft Actuators," *Advanced Intelligent Systems* 4, no. 10 (2022): 2200122, https://doi.org/10.1002/aisy.202200122.

12. W. Heng, S. Solomon, and W. Gao, "Flexible Electronics and Devices as Human–Machine Interfaces for Medical Robotics," *Advanced Materials* 34, no. 16 (2022): 2107902, https://doi.org/10.1002/adma.202107902.

13. R. S. Dahiya, G. Metta, M. Valle, and G. Sandini, "Tactile Sensing—From Humans to Humanoids," *IEEE Transactions on Robotics* 26, no. 1 (2010): 1–20, https://doi.org/10.1109/TRO.2009.2033627.

14. Y. Mengüç, Y.-L. Park, H. Pei, et al., "Wearable Soft Sensing Suit for Human Gait Measurement," *International Journal of Robotics Research* 33, no. 14 (2014): 1748–1764, https://doi.org/10.1177/0278364914543793.

15. P. Polygerinos, Z. Wang, K. C. Galloway, R. J. Wood, and C. J. Walsh, "Soft Robotic Glove for Combined Assistance and at-Home Rehabilitation," *Robotics and Autonomous Systems* 73 (2015): 135–143, https://doi.org/10.1016/j.robot.2014.08.014.

16. J. Amend, N. Cheng, S. Fakhouri, and B. Culley, "Soft Robotics Commercialization: Jamming Grippers From Research to Product," *Soft Robotics* 3, no. 4 (2016): 213–222, https://doi.org/10.1089/soro.2016.0021.

17. M. A. Robertson, H. Sadeghi, J. M. Florez, and J. Paik, "Soft Pneumatic Actuator Fascicles for High Force and Reliability," *Soft Robotics* 4, no. 1 (2017): 23–32, https://doi.org/10.1089/soro.2016.0029.

18. R. S. Johansson and A. B. Vallbo, "Tactile Sensibility in the Human Hand: Relative and Absolute Densities of Four Types of Mechanoreceptive Units in Glabrous Skin," *Journal of Physiology* 286, no. 1 (1979): 283–300, https://doi.org/10.1113/jphysiol.1979.sp012619.

19. J. Su, J. M. R. Tan, J. Liu, et al., "Bioarchitectonics-Inspired Soft Grippers With Cutaneous Slip Perception," *Science Advances* 11, no. 33 (2025): eadx4206, https://doi.org/10.1126/sciadv.adx4206.

29439973, 0, Downloaded from https://advanced.onlinelibrary.wiley.com/doi/10.1002/adrr.70186 by NICE, National Institute for Health and Care Excellence, Wiley Online Library on [07/11/2026]. See the Terms and Conditions (https://onlinelibrary.wiley.com/terms-and-conditions) on Wiley Online Library for rules of use; OA articles are governed by the applicable Creative Commons License

20. W. Diao, X. Wang, W. Shi, Y. Cao, and G. Liu, "A Tribo-Piezoelectric Coupled Sensor for Force and Slip Detection in Soft Grippers," *Nano Energy* 136 (2025): 110697, https://doi.org/10.1016/j.nanoen.2025.110697.

21. H. Yang, Y. Chen, Y. Sun, and L. Hao, "A Novel Pneumatic Soft Sensor for Measuring Contact Force and Curvature of a Soft Gripper," *Sensors and Actuators A: Physical* 266 (2017): 318–327, https://doi.org/10.1016/j.sna.2017.09.040.

22. B. G. Ki and Y.-J. Park, "Soft Gripper With Movable Variable Stiffness Mechanism and Embedded Soft Sensors for Adaptive Grasping Strategies," *IEEE Robotics and Automation Letters* 10, no. 3 (2025): 2710–2717, https://doi.org/10.1109/LRA.2025.3534058.

23. Y. Hao, Z. Liu, J. Liu, et al., "A Soft Gripper With Programmable Effective Length, Tactile and Curvature Sensory Feedback," *Smart Materials and Structures* 29, no. 3 (2020): 035006, https://doi.org/10.1088/1361-665X/ab6759.

24. B. S. Homberg, R. K. Katzschmann, M. R. Dogar, and D. Rus, "Robust Proprioceptive Grasping With a Soft Robot Hand," *Autonomous Robots* 43, no. 3 (2019): 681–696, https://doi.org/10.1007/s10514-018-9754-1.

25. R. L. Truby, R. K. Katzschmann, J. A. Lewis, and D. Rus, "Soft Robotic Fingers With Embedded Ionogel Sensors and Discrete Actuation Modes for Somatosensitive Manipulation," in *2019 2nd IEEE International Conference on Soft Robotics (RoboSoft)* (IEEE, 2019), 322–329, https://doi.org/10.1109/ROBOSOFT.2019.8722722.

26. H. Zhao, K. O'Brien, S. Li, and R. F. Shepherd, "Optoelectronically Innervated Soft Prosthetic Hand via Stretchable Optical Waveguides," *Science Robotics* 1, no. 1 (2016): eaai7529, https://doi.org/10.1126/scirobotics.aai7529.

27. A. K. Mishra, A. Ramaswami, V. Shree, et al., "Sensor Fusion of Touch & Vision in Soft Manipulators for Fruit Picking," *Nature Communications* 17, no. 1 (2026): 4370, https://doi.org/10.1038/s41467-026-70588-9.

28. Y. Fan, C. Zhang, Y. Ying, et al., "Intelligent Soft Robotic Gripper for Non-Destructive Grasping and Attribute Recognition via Multi-Modal Waveguide Tactile Sensors," *Microsystems & Nanoengineering* 12, no. 1 (2026): 233, https://doi.org/10.1038/s41378-026-01364-4.

29. H. Wu, C. Tang, Y. Peng, et al., "Shape and Tactile Perceptions of Soft Fingers via Distributed Curvature Sensing for Intelligent Grippers," *Soft Robotics* 13, no. 3 (2026): 21695172261417888, https://doi.org/10.1177/21695172261417888.

30. J. B. Chossat, Y. L. Park, R. J. Wood, and V. Duchaine, "A Soft Strain Sensor Based on Ionic and Metal Liquids," *IEEE Sensors Journal* 13, no. 9 (2013): 3405–3414, https://doi.org/10.1109/JSEN.2013.2263797.

31. R. D. Ponce Wong, J. D. Posner, and V. J. Santos, "Flexible Microfluidic Normal Force Sensor Skin for Tactile Feedback," *Sensors and Actuators A: Physical* 179 (2012): 62–69, https://doi.org/10.1016/j.sna.2012.03.023.

32. J. Chen, J. Zhang, Z. Luo, et al., "Superelastic, Sensitive, and Low Hysteresis Flexible Strain Sensor Based on Wave-Patterned Liquid Metal for Human Activity Monitoring," *ACS Applied Materials & Interfaces* 12 (2020): 22200, https://doi.org/10.1021/acsami.0c04709.

33. B. C.-K. Tee, C. Wang, R. Allen, and Z. Bao, "An Electrically and Mechanically Self-Healing Composite With Pressure- and Flexion-Sensitive Properties for Electronic Skin Applications," *Nature Nanotechnology* 7, no. 12 (2012): 825–832, https://doi.org/10.1038/nnano.2012.192.

34. M. Amjadi, Y. J. Yoon, and I. Park, "Ultra-Stretchable and Skin-Mountable Strain Sensors Using Carbon Nanotubes–Ecoflex Nanocomposites," *Nanotechnology* 26, no. 37 (2015): 375501, https://doi.org/10.1088/0957-4484/26/37/375501.

35. A. Koivikko, V. Lampinen, M. Pihlajamäki, K. Yiannacou, V. Sharma, and V. Sariola, "Integrated Stretchable Pneumatic Strain Gauges for Electronics-Free Soft Robots," *Communications Engineering* 1, no. 1 (2022): 1–10, https://doi.org/10.1038/s44172-022-00015-6.

36. R. L. Truby, L. Chin, A. Zhang, and D. Rus, "Fluidic Innervation Sensorizes Structures From a Single Build Material," *Science Advances* 8, no. 32 (2022): eabq4385, https://doi.org/10.1126/sciadv.abq4385.

37. D. Gong, R. He, J. Yu, and G. Zuo, "A Pneumatic Tactile Sensor for Co-Operative Robots," *Sensors* 17, no. 11 (2017): 2592, https://doi.org/10.3390/s17112592.

38. C. Tawk, H. Zhou, E. Sariyildiz, M. In Het Panhuis, G. M. Spinks, and G. Alici, "Design, Modeling, and Control of a 3D Printed Monolithic Soft Robotic Finger With Embedded Pneumatic Sensing Chambers," *IEEE/ASME Transactions on Mechatronics* 26, no. 2 (2021): 876–887, https://doi.org/10.1109/TMECH.2020.3009365.

39. P. Rothemund, A. Ainla, L. Belding, et al., "A Soft, Bistable Valve for Autonomous Control of Soft Actuators," *Science Robotics* 3, no. 16 (2018): eaar7986, https://doi.org/10.1126/scirobotics.aar7986.

40. S. Zou, S. Picella, J. de Vries, V. G. Kortman, A. Sakes, and J. T. B. Overvelde, "A Retrofit Sensing Strategy for Soft Fluidic Robots," *Nature Communications* 15, no. 1 (2024): 539, https://doi.org/10.1038/s41467-023-44517-z.

41. V. Lampinen, A. Koivikko, M. Pihlajamäki, V. Sharma, and V. Sariola, "Soft Pneumatic Tactile Pressure Sensor Matrix," *Robotics Reports* 2, no. 1 (2024): 115–127, https://doi.org/10.1089/rorep.2024.0034.

42. V. Lampinen, M. Pihlajamäki, A. Koivikko, and V. Sariola, "Soft Micropneumatic Touchpad," *Advanced Intelligent Systems* 7, no. 2 (2024): 2400381, https://doi.org/10.1002/aisy.202400381.

43. W. Dou, G. Zhong, J. Cao, Z. Shi, B. Peng, and L. Jiang, "Soft Robotic Manipulators: Designs, Actuation, Stiffness Tuning, and Sensing," *Advanced Materials Technologies* 6, no. 9 (2021): 2100018, https://doi.org/10.1002/admt.202100018.

44. J. Shintake, V. Cacucciolo, D. Floreano, and H. Shea, "Soft Robotic Grippers," *Advanced Materials* 30, no. 29 (2018): 1707035, https://doi.org/10.1002/ADMA.201707035.

45. J. Hughes, U. Culha, F. Giardina, F. Guenther, A. Rosendo, and F. Iida, "Soft Manipulators and Grippers: A Review," *Frontiers in Robotics and AI* 3 (2016): 69, https://doi.org/10.3389/frobt.2016.00069.

46. H. Wang, M. Totaro, and L. Beccai, "Toward Perceptive Soft Robots: Progress and Challenges," *Advanced Science* 5, no. 9 (2018): 1800541, https://doi.org/10.1002/advs.v5.9.

47. Z. Zhou, R. Zuo, B. Ying, et al., "A Sensory Soft Robotic Gripper Capable of Learning-Based Object Recognition and Force-Controlled Grasping," *IEEE Transactions on Automation Science and Engineering* 21, no. 1 (2024): 844–854, https://doi.org/10.1109/TASE.2022.3228255.

48. T. Jin, Z. Sun, L. Li, et al., "Triboelectric Nanogenerator Sensors for Soft Robotics Aiming at Digital Twin Applications," *Nature Communications* 11, no. 1 (2020): 5381, https://doi.org/10.1038/s41467-020-19059-3.

49. A. Zhang, L. Chin, D. L. Tong, and D. Rus, "Embedded Air Channels Transform Soft Lattices into Sensorized Grippers," in *2024 IEEE International Conference on Robotics and Automation (ICRA)* (IEEE, 2024), 5264–5270.

50. O. Shorthose, A. Albini, L. He, and P. Maiolino, "Design of a 3D-Printed Soft Robotic Hand With Integrated Distributed Tactile Sensing," *IEEE Robotics and Automation Letters* 7, no. 2 (2022): 3945–3952, https://doi.org/10.1109/LRA.2022.3149037.

51. Y. L. Park, B. R. Chen, and R. J. Wood, "Design and Fabrication of Soft Artificial Skin Using Embedded Microchannels and Liquid Conductors," *IEEE Sensors Journal* 12, no. 8 (2012): 2711–2718, https://doi.org/10.1109/JSEN.2012.2200790.

52. National Instruments, "Measuring Strain with Strain Gages," accessed: 3.9.2026, https://www.ni.com/en/shop/data-acquisition/sensor-fundamentals/measuring-strain-with-strain-gages.html.

53. S. Wang, H. Zhen, S. Duan, and X. Sha, "Fluidic Feedback for Soft Actuators: An Electronic-Free System for Sensing and Control,"

29439973, 0, Downloaded from https://advanced.onlinelibrary.wiley.com/doi/10.1002/adrr.70186 by NICE, National Institute for Health and Care Excellence, Wiley Online Library on [07/11/2026]. See the Terms and Conditions (https://onlinelibrary.wiley.com/terms-and-conditions) on Wiley Online Library for rules of use; OA articles are governed by the applicable Creative Commons License

Bioinspiration & Biomimetics 20, no. 1 (2024): 016025, https://doi.org/10.1088/1748-3190/ad9f02.

54. A. Goshtasbi, S. P. Murali Babu, R. Moreira, et al., "AI-Infused Soft Fluidic Tactile Sensing," in *2024 IEEE 7th International Conference on Soft Robotics (RoboSoft)* (IEEE, 2024), 1095–1100.

55. D. P. Holland, E. J. Park, P. Polygerinos, G. J. Bennett, and C. J. Walsh, "The Soft Robotics Toolkit: Shared Resources for Research and Design," *Soft Robotics* 1, no. 3 (2014): 224–230, https://doi.org/10.1089/soro.2014.0010.

Supporting Information

Additional supporting information can be found online in the Supporting Information section.

29439973, 0, Downloaded from https://advanced.onlinelibrary.wiley.com/doi/10.1002/adrr.70186 by NICE, National Institute for Health and Care Excellence, Wiley Online Library on [07/11/2026]. See the Terms and Conditions (https://onlinelibrary.wiley.com/terms-and-conditions) on Wiley Online Library for rules of use; OA articles are governed by the applicable Creative Commons License